Artificial Dissipation Models for the Euler Equations

Thomas H. Pulliam*
NASA Ames Research Center, Moffett Field, California

Various artificial dissipation models that are used with central difference algorithms for the Euler equations are analyzed for their effect on accuracy, stability, and convergence rates. In particular, linear and nonlinear models are investigated using an implicit approximate factorization code (ARC2D) for transonic airfoils. Fully implicit application of the dissipation models is shown to improve robustness and convergence rates. The treatment of dissipation models at boundaries will be examined. It will be shown that accurate, error free solutions with sharp shocks can be obtained using a central difference algorithm coupled with an appropriate nonlinear artificial dissipation model.

I. Introduction

THE solution of the Euler equations using numerical techniques requires the use of either a differencing method with inherent dissipation or the addition of dissipation terms to a nondissipative scheme. This is because the Euler equations do not provide any natural dissipation mechanism (such as viscosity in the Navier-Stokes equations) that would eliminate high frequencies which are caused by nonlinearities and especially shocks. A variety of numerical algorithms and computer codes for the Euler equations have been developed. Methods such as MacCormack's[1] explicit scheme and Steger's[2] application of the Beam and Warming[3] implicit algorithm are in wide use. Some notable recent developments based on explicit Runge-Kutta schemes are the work of Jameson et al.[4] and Rizzi and Eriksson.[5] The time integration scheme, boundary condition treatment, and other details are different from method to method. These all have one thing in common: The use of a basically central difference approximation to the spatial derivatives and the addition of some form of artificial dissipation. In contrast there is a currently popular class of schemes, [monotone, total variation diminishing (TVD), flux split, flux difference, lambda] that employ some form of upwind differencing under the assumptions of characteristic theory and wave propagation. The work of Steger and Warming,[6] Roe,[7] Van Leer,[8] Osher and Chakravarthy,[9] and Harten's TVD methods[10] all fall in this category. Although it will not be shown here for every case, these schemes are all equivalent to a central differencing scheme plus some form of dissipation.

The addition of artificial dissipation to central differencing will be the focus of this paper. It is added for two main reasons: first, to control the odd-even uncoupling of grid points typical of central differencing and, second, to control strong nonlinear effects such as shocks. The paper investigates various forms of artificial dissipation employed in the Euler codes. The particular difference forms and theory behind the choice of coefficient will be examined here, as well as some stability and accuracy arguments when possible.

Results for flow over airfoils with shocks will be used as test cases. A recent version of Steger's[2] two-dimensional implicit central difference scheme described in Refs. 11 and 12 will be used as the test code. The dissipation models discussed here have been applied in viscous computations, but will not be addressed in this paper. In particular, the interest is in evaluating the effect of the artificial dissipation on the accuracy and stability of fluid dynamic results.

Presented as Paper 85-0438 at the AIAA 23rd Aerospace Sciences Meeting, Reno, NV, Jan. 14-17, 1985; received May 10, 1985; revision received March 17, 1986.

*Research Scientist, Computational Fluid Dynamics Branch. Member AIAA.

II. Two-Dimensional Euler Equations

Much of the development of the equations and algorithm used here is available from other sources (see Refs. 2, 3, 11, and 12. Just the aspects important to the current developments are presented here.

The two-dimensional Euler equations can be transformed from Cartesian coordinates to general curvilinear coordinates where

$$\tau = t \qquad \xi = \xi(x,y,t) \qquad \eta = \eta(x,y,t) \tag{1}$$

The Euler equations written in generalized coordinates are

$$\partial_\tau \hat{Q} + \partial_\xi \hat{E} + \partial_\eta \hat{F} = 0 \tag{2}$$

$$\hat{Q} = J^{-1}\begin{bmatrix} \rho \\ \rho u \\ \rho v \\ e \end{bmatrix}, \quad \hat{E} = J^{-1}\begin{bmatrix} \rho U \\ \rho u U + \xi_x p \\ \rho v U + \xi_y p \\ U(e+p) - \xi_t p \end{bmatrix}$$

$$\hat{F} = J^{-1}\begin{bmatrix} \rho V \\ \rho u V + \eta_x p \\ \rho v V + \eta_y p \\ V(e+p) - \eta_t p \end{bmatrix}$$

where

$$U = \xi_t + \xi_x u + \xi_y v \qquad V = \eta_t + \eta_x u + \eta_y v$$

are the contravariant velocities. Pressure is related to the conservative flow variables Q by the equation of state

$$p = (\gamma - 1)\left[e - \tfrac{1}{2}\rho(u^2 + v^2)\right] \tag{3}$$

where γ is the ratio of specific heats, generally taken as 1.4. The speed of sound $a = \sqrt{\gamma p/\rho}$. The ($\hat{}$) is dropped for simplicity of notation except where noted.

The metric terms are related to derivatives of x, y, and t by

$$\xi_x = Jy_\eta \qquad \xi_y = -Jx_\eta \qquad \xi_t = -x_\tau \xi_x - y_\tau \xi_y$$
$$\eta_x = -Jy_\xi \qquad \eta_y = Jx_\xi \qquad \eta_t = -x_\tau \eta_x - y_\tau \eta_y$$
$$J = 1/(x_\xi y_\eta - x_\eta y_\xi) \tag{4}$$

A commonly used element of the Euler equations are the flux Jacobians

$$E = AQ \qquad F = BQ \tag{5}$$

with $A = \partial E/\partial Q$ and $B = \partial F/\partial Q$.

The flux Jacobians A and B each have real eigenvalues and a complete set of eigenvectors. Therefore, the Jacobian matrices can be diagonalized (see Ref. 13) as

$$\Lambda_A = T_\xi^{-1} A T_\xi \qquad \Lambda_B = T_\eta^{-1} B T_\eta \tag{6}$$

with T_ξ the matrix whose columns are the eigenvectors of A, and T_η the corresponding eigenvector matrix for B (see Ref. 11). The eigenvalue matrices are

$$\Lambda_A = \begin{bmatrix} U & 0 & 0 & 0 \\ 0 & U & 0 & 0 \\ 0 & 0 & U + a\sqrt{\xi_x^2 + \xi_y^2} & 0 \\ 0 & 0 & 0 & U - a\sqrt{\xi_x^2 + \xi_y^2} \end{bmatrix}$$
$$\Lambda_b = \begin{bmatrix} V & 0 & 0 & 0 \\ 0 & V & 0 & 0 \\ 0 & 0 & V + a\sqrt{\eta_x^2 + \eta_y^2} & 0 \\ 0 & 0 & 0 & V - a\sqrt{\eta_x^2 + \eta_y^2} \end{bmatrix} \tag{7}$$

III. Central Differencing

For now ignore the time-stepping procedure and examine only the steady part of the Euler equations. Introducing mesh points j,k, variables can be defined at mesh point as

$$u_{j,k} := u(j\Delta\xi, k\Delta\eta) \tag{8}$$

The spatial derivatives $\partial_\xi E$ and $\partial_\eta F$ can be approximated by second-order central differences of the form

$$\delta_\xi E_{j,k} = \frac{E_{j+1,k} - E_{j-1,k}}{2\Delta\xi} \qquad \delta_\eta F_{j,k} = \frac{F_{j,k+1} - F_{j,k-1}}{2\Delta\eta} \tag{9}$$

Finite volume formulations (see Refs. 4 or 5) can be cast into very similar forms.

The details and effects of the physical boundary conditions are avoided for now and it is assumed that they are applied in a consistent, stable, and accurate fashion. Ignoring the effect of numerical boundary conditions, it is well-known that central differencing provides no mechanism for dissipation. It is also well-known that central differencing naturally uncouples grid points in an odd-even fashion. It can be shown that, even for linear constant coefficient problems, inaccuracies or inconsistencies at boundaries can excite oscillations. These oscillations can be controlled by artificial dissipation or by proper boundary condition treatment. Recent work by Liu[14] and Liu and Lomax[15] demonstrates methods that use pure central differencing without artificial dissipation where they link the proper treatment of boundaries and the concept of the two solution families from the natural odd-even uncoupling. They have also successfully applied their methods to flows with shocks for the one-dimensional Euler equations and are presently extending their work to two-dimensions.

Two aspects of current solution techniques for the Euler equations using central differencing methods require the addition of some form of artificial dissipation. Even starting with a smooth solution, nonlinearity can continuously excite the odd-even uncoupling and dissipation can be used to control this. Of more interest though is the action of specific nonlinear effects, such as shocks in transonic flow. In the absence of true viscosity (i.e., the Euler equations), shocks are sharp discontinuities in the flow. From the point of view of a Fourier analysis, an infinite number of modes are needed to resolve a discontinuity. The disparity between the physical problem and its discrete representation necessitates dissipation of unresolvable modes. Without such dissipation these unresolved modes appear as error (aliasing) in the resolvable modes, degrading the accuracy and stability of the computations. The particular nature, amount, and form of this dissipation will determine the accuracy and reliability of a solution.

It is interesting to look back to the pioneering work of Von Neumann and Richtmyer[16] in which they "introduce (artificial) dissipative terms into the equations so as to give shocks a thickness comparable to...the spacing of the points in the network." In their paper they go on to develop a dissipation model in the form of a nonlinear viscosity and show that the resulting equations satisfy the Rankine-Hugoniot relations, while having a negligible effect outside the shock region.

IV. Upwind Connection to Artificial Dissipation

In the last few years a number of schemes have been developed based on upwind differencing. The flux split schemes of Steger and Warming,[6] Roe,[7] and Van Leer[8] employ a decomposition of the flux vectors in such a way that each element can be stably differenced in an upwind fashion. Other schemes of a similar nature but based on more complicated theories are the flux difference scheme of Osher and Chakravarthy[9] and Harten's TVD methods.[10] These schemes all claim (with good justification) to be physically consistent since they follow in some sense the characteristics of the flow. They in general can be shown to produce sharp shocks without added dissipation or stability restrictions. They are complicated schemes though, which are just now being applied to complicated flowfield situations. These schemes have an inherent amount of internal dissipation, due to the one-sided differences, which is usually difficult to modify or decrease. It may be advantageous to have instead the flexibility and simplicity of a central difference scheme with a controllable amount of artificial dissipation.

It can be shown that upwind schemes have an equivalence to central difference schemes with added dissipation. The central schemes are much simpler and more flexible and are therefore desirable if the dissipation can be added in an analogous fashion to the upwind schemes. In fact, upwind schemes can be used to guide the development of nonoscillatory, robust, and efficient artificial dissipation schemes.

The plus-minus flux split method of Steger and Warming[6] will be used here to demonstate the dissipative nature of upwind schemes. The approach taken is to split the eigenvalue matrix Λ of the flux Jacobians into two matrices, one with all positive elements and the other with all negative elements. Then the similarity transformations T_ξ or T_η are used to form new matrices A^+, A^- and B^+, B^-. Formally,

$$A = T_\xi \Lambda_A T_\xi^{-1} = T_\xi (\Lambda_A^+ + \Lambda_A^-) T_\xi^{-1} = A^+ + A^- \tag{10a}$$

with

$$\Lambda_A^{\pm} = \frac{\Lambda_A \pm |\Lambda_A|}{2} \tag{10b}$$

Here, $|\Lambda|$ represents the absolute values of the elements of Λ. The two matrices, A^+ and A^-, have by construction all positive and all negative eigenvalues, respectively.

New flux vectors can be constructed as

$$\begin{aligned} E &= AQ = (A^+ + A^-)Q = E^+ + E^- \\ F &= BQ = (B^+ + B^-)Q = F^+ + F^- \end{aligned} \tag{11}$$

Different types of spatial differencing can now be used for each of the new flux vectors. One stable form is to use one-sided backward differencing for the positive terms and one-sided forward differencing for the negative terms. The one-sided difference operators are usually either first-order accurate

$$\nabla_\xi^b u_{j,k} = \frac{u_{j,k} - u_{j-1,k}}{\Delta\xi} \qquad \Delta_\xi^f u_{j,k} = \frac{u_{j+1,k} - u_{j,k}}{\Delta\xi} \tag{12a}$$

or second-order accurate

$$\begin{aligned} \delta_\xi^b u_{j,k} &= \frac{3/2u_{j,k} - 2u_{j-1,k} + 1/2u_{j-2,k}}{\Delta\xi} \\ \delta_\xi^f u_{j,k} &= \frac{-3/2u_{j,k} + 2u_{j+1,k} - 1/2u_{j+2,k}}{\Delta\xi} \end{aligned} \tag{12b}$$

Similar expressions are used for the η derivatives. Note that $\Delta\xi = 1$, but it will appear in formulas where its presence conveys meaning.

The plus-minus matrices A^+ and A^- can be written as

$$A^{\pm} = T_\xi \left(\frac{\Lambda \pm |\Lambda|}{2} \right) T_\xi^{-1} = \frac{A \pm |A|}{2} \tag{13a}$$

which gives

$$E^{\pm} = A^{\pm} Q = \frac{A}{2} Q \pm \frac{|A|}{2} Q = \frac{E}{2} \pm \frac{|A|}{2} Q \tag{13b}$$

Similar expressions are obtainable for the B matrix and flux vector F.

Examining the flux derivative

$$\delta_\xi^b E^+ + \delta_\xi^f E^- \tag{14a}$$

where second-order one-sided difference approximations are chosen

$$\delta_\xi^b = \frac{3I - 4\mathcal{E}^{-1} + \mathcal{E}^{-2}}{2\Delta\xi} \qquad \delta_\xi^f = \frac{-3I + 4\mathcal{E}^{+1} - \mathcal{E}^{+2}}{2\Delta\xi} \tag{14b}$$

with $\mathcal{E}^i$ the shift operator, i.e., $\mathcal{E}^{\pm i} u_j = u_{j\pm i}$ and combining Eq. (13b) and Eqs. (14a) and (14b) produces

$$\tfrac{1}{2}[(\delta_\xi^b + \delta_\xi^f)E + (\delta_\xi^b - \delta_\xi^f)|A|Q] \tag{15}$$

for the difference equation (14a)

It is easily shown that

$$\frac{\delta_\xi^b + \delta_\xi^f}{2} = \frac{-\mathcal{E}^{+2} + 4\mathcal{E}^{+1} - 4\mathcal{E}^{-1} + \mathcal{E}^{-2}}{4\Delta\xi} = \bar{\delta}_\xi \tag{16a}$$

which is a second-order central difference approximation for the spatial derivative δ_ξ. The other term of Eq. (15) is of more interest, where

$$\begin{aligned} \frac{\delta_\xi^b - \delta_\xi^f}{2} &= \frac{\mathcal{E}^{+2} - 4\mathcal{E}^{+1} + 6I - 4\mathcal{E}^{-1} + \mathcal{E}^{-2}}{4\Delta\xi} \\ &= \frac{1}{4\Delta\xi} (\Delta_\xi \nabla_\xi)^2 \end{aligned} \tag{16b}$$

which is a fourth-difference formula. The difference operators are

$$\begin{aligned} \nabla_\xi q_{j,k} &= q_{j,k} - q_{j-1,k} \qquad & \Delta_\xi q_{j,k} &= q_{j+1,k} - q_{j,k} \\ \nabla_\eta q_{j,k} &= q_{j,k} - q_{j,k-1} \qquad & \Delta_\eta q_{j,k} &= q_{j,k+1} - q_{j,k} \end{aligned} \tag{17}$$

Note that these are difference operators and are not intended to represent approximations to spatial derivatives.

Now Eq. (15) can be written as

$$\left(\delta_\xi E + \frac{1}{4\Delta\xi} (\Delta_\xi \nabla_\xi)^2 |A| Q \right) \tag{18a}$$

The form now is a second-order central difference plus a fourth-difference dissipation. The dissipative term is a natural consequence of the upwind differencing. It is interesting to note that the central difference term, Eq. (16a), is not the standard three-point difference. If first-order formulas are employed for the upwind differences, then a similar analysis would produce the standard second-order three-point central differencing plus a second-difference dissipative. For instance, Eq. (18a) is replaced by

$$\left(\delta_\xi E - \frac{1}{2\Delta\xi} (\Delta_\xi \nabla_\xi) |A| Q \right) \tag{18b}$$

Examining Eqs. (18) can guide the development of artificial dissipation models for central difference schemes. Adding fourth-difference dissipation to a central difference produces the equivalent of a second-order upwind scheme. The use of second-difference dissipation can produce a first-order upwind equivalent. Recent work applying flux limiters to upwind schemes and TVD concepts suggests that the best approach for an upwind algorithm is to use a locally first-order upwind difference at a shock and second-order elsewhere. This can be accomplished by switching and transitioning of second-difference and fourth-difference dissipation added to a central scheme. The coefficients for the dissipation parts of Eq. (18) suggest some sort of flux Jacobian scaling where, for instance, a spectral radius of the Jacobians could be used.

V. Implicit Algorithm and Constant Coefficient Dissipation

The implicit approximate factorization algorithm developed by Beam and Warming[3] and Steger[2] has the form

$$\begin{aligned} &[I + h\delta_\xi \hat{A}^n + D_\xi^{(2)}][I + h\delta_\eta \hat{B}^n + D_\eta^{(2)}]\Delta\hat{Q}^n \\ &\quad = -h[\delta_\xi \hat{E}^n + \delta_\eta \hat{F}^n - D^{(4)}] = \hat{R}^n \end{aligned} \tag{19}$$

where the explicit fourth-difference dissipation

$$D^{(4)} = -\epsilon_e \Delta t J^{-1}[(\nabla_\xi \Delta_\xi)^2 + (\nabla_\eta \Delta_\eta)^2] J\hat{Q}^n \tag{20a}$$

is added and implicit second-difference dissipation

$$D_\xi^{(2)} = -\epsilon_i \Delta t J^{-1} \nabla_\xi \Delta_\xi J \qquad D_\eta^{(2)} = -\epsilon_i \Delta t J^{-1} \nabla_\eta \Delta_\eta J \tag{20b}$$

is inserted into the implicit operators. The parameter ϵ_e is chosen to be $O(1)$ and $\epsilon_i = 2\epsilon_e$. The smoothing terms are scaled with Δt which makes the steady state independent of the time step. It is important to realize that these added terms modify the original partial differential equations and the coefficients used should be kept as small as possible while still maintaining stability. Typically, it is a matter of experience which decides the values for the coefficients for a particular application.

The dissipation terms defined by Eqs. (20) include the metric Jacobian J in such a way that the dissipation acts upon the unscaled Q and not $\hat{Q}$. This is done so that the dissipation is not directly influenced by the grid distribution since smooth functions Q may occur in regions of rapid mesh variation. The scaling of the terms by J^{-1} makes the equations consistent with the flux derivatives and time derivative. Also note that the dissipation terms do not include the mesh cell $\Delta\xi$ or $\Delta\eta$. These terms are treated as difference operators and not direct approximations to function derivatives (although they have some correspondence). That is, the dissipation should be thought of as a difference stencil applied to the function and not a derivative of the function. Therefore, reference to a fourth-difference dissipation corresponds to equations of the form of Eq. (20a) and second-difference dissipation to equations of the form of Eq. (20b).

The fourth-difference dissipation was added to the basic algorithm to control nonlinear instabilities. The second-difference implicit dissipation is added to stabilize the explicit fourth-difference for large coefficient $\Delta t\epsilon_e$. Linear analysis shows that, if the implicit coefficient ϵ_i is chosen to be larger than the explicit coefficient ϵ_e, unconditionally linear stability results (see Sec. VIII). A sufficient relation is $\epsilon_i = 2\epsilon_e$. Note the parallelism between Eqs. (18) and (20). The fourth-difference dissipation can be viewed as an attempt to bias the differencing scheme in a second-order upwind fashion. The implicit dissipation produces a bias similar to a first-order upwind scheme. The main difference between an upwind scheme and the use of added dissipation terms lies in the choice of coefficients.

A calculation using this algorithm for transonic flow about a NACA 0012 airfoil at a Mach number $M_\infty = 0.8$ and angle of attack $\alpha = 1.25$ deg is shown in Fig. 1. The solution was converged to machine zero and was stable throughout the integration, in this case $\epsilon_e = 1.0$ and $\epsilon_i = 2.0$. While these values were large enough to maintain stability, they still did not eliminate the obvious oscillations in the preshock and postshock regions. Shown in Fig. 2 are pressure contours in the flowfield which indicate that the oscillations extend above the body into the flow. The mesh used for this case was clustered in the shock regions, see Fig. 3. As can be seen the oscillations are of the highest frequency obtainable on the mesh and increased clustering would show higher frequency oscillations while reduced clustering would reduce them. Larger values of the dissipation coefficients can modulate the oscillations but not eliminate them completely without destroying shock resolution. The overall accuracy of this calculation is quite good except for the oscillations. In fact, a cosmetic averaging of the pressure at the body would produce a very acceptable solution. It is preferred though to modify the dissipation terms or the differencing scheme to produce an automatic mechanism for calculating accurate solutions.

VI. Upwind Differencing in Supersonic Regions Only

Central differences can be combined with upwind schemes to produce better shock capturing capabilities. The use of upwinding for shocks is widespread in transonic potential calculations. Upwind differencing before shocks can have a stabilizing effect by eliminating oscillations associated with central differencing and it can also improve the accuracy of the calculations by sharpening shock profiles. The particular form of upwinding is taken from Warming and Beam,[17] was employed in the original work of Steger,[2] and also described in Ref. 18. For airfoil calculations where the ξ coordinate is locally aligned with the surface, upwind differencing is applied in the ξ direction by replacing δ_ξ in Eq. (19) with

$$\tilde{\delta}_\xi = \frac{I - \tilde{\nabla}_\xi \epsilon_j}{\tfrac{1}{2}(2I - \epsilon_j I + \mathcal{E}^- \epsilon_j)} \delta_\xi^c \tag{21a}$$

with $\tilde{\nabla}_\xi = I - \mathcal{E}^{-\frac{1}{2}}$ and the central difference operator rewritten as

$$\delta_\xi^c = \frac{\mathcal{E}^{+\frac{1}{2}} - \mathcal{E}^{-\frac{1}{2}}}{\Delta\xi} \qquad \mathcal{E}^{\pm\frac{1}{2}} = \frac{I + \mathcal{E}^{\pm}}{2} \tag{21b}$$

Note that Eqs. (21) is in operator notation and is actually implemented by clearing the denominator, which then operates on the other terms in Eq. (19). This particular form transitions from central to upwind and back to central differencing such that conservation is maintained.

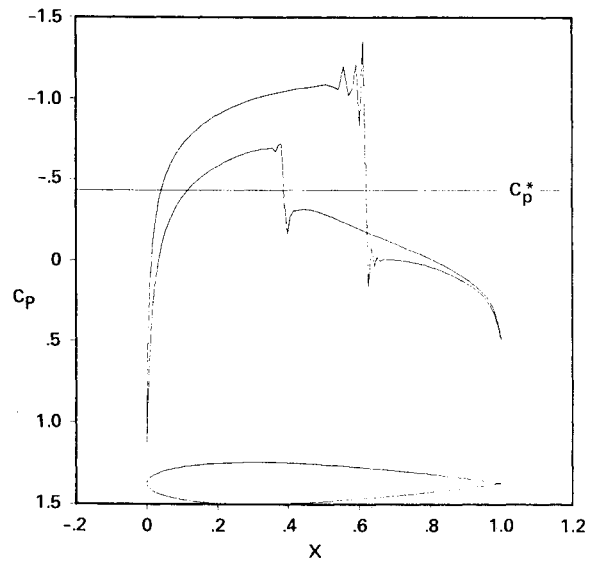

Fig. 1 Coefficient of pressure showing central difference oscillations at shock.

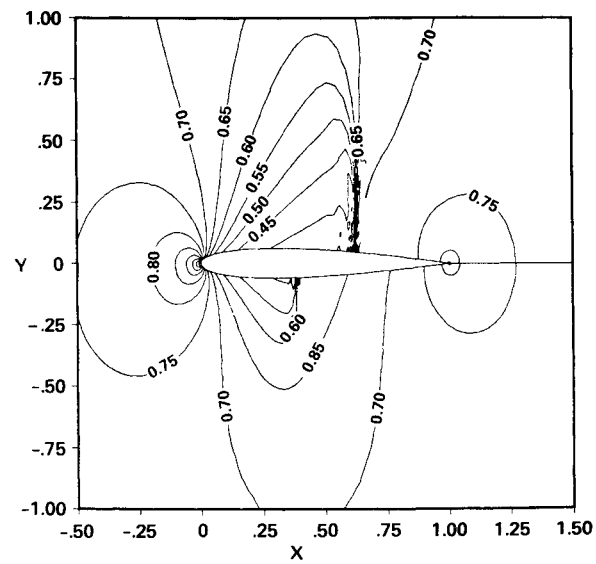

Fig. 2 Pressure field showing extent of oscillations.

This new differencing depends on the two parameters $(\epsilon_{j-1},\epsilon_j)$ and there are four possible cases:

$$(\epsilon_{j-1},\epsilon_j)=\begin{bmatrix}(0,0) & \text{purely central differencing}\\ (1,1) & \text{purely upwind differencing}\\ (0,1) & \text{transition from central to upwind}\\ (1,0) & \text{transition from upwind to central}\end{bmatrix} \tag{22}$$

The parameter ϵ_j is chosen to be 0 in subsonic regions and 1 in supersonic regions. The eigenvalues of the Jacobian matrix $\hat{A}$ are $U,U,U\pm a\sqrt{\xi_x^2+\xi_y^2}$. These are checked along each line of integration and ϵ_j is set to 1 when all the eigenvalues are positive for $U>0$ or negative for $U<0$. Note that this is not strictly subsonic or supersonic flow, but rather a condition based on the characteristic directions of the flow.

It is also necessary to switch off the added dissipation terms, Eq. (20a), in the upwinded areas. The addition of the fourth-difference smoothing has been found to be detrimental and not necessary due to the dissipative nature of the backward and forward difference operators used in the supersonic regions. The fourth-difference ξ terms of Eq. (20a) are modified to

$$[(\nabla_\xi-\nabla_\xi\epsilon_j)\Delta_\xi\nabla_\xi\Delta_\xi]=[(1-\epsilon_j)-(1-\epsilon_{j-1})\mathcal{E}^-][\mathcal{E}^{+2}-3\mathcal{E}^++3I-\mathcal{E}^-] \tag{23}$$

An example of the effect of using this new differencing scheme on the previous case is shown in Fig. 4. Here the preshock oscillations are eliminated except for a one-point overshoot at the strong upper surface shock. This can be traced to the transition operator and could be eliminated by adjusting the values of ϵ_j. The postshock oscillations are still evident because the scheme reverts to the central operators in the subsonic regions. Pressure contours are shown in Fig. 5 and compare quite well (except for the oscillation detail) with Fig. 2.

Besides the distasteful oscillations which are still evident for this scheme, there are other disadvantages to this method. The logic involved in choosing the coefficient ϵ_j is rather complicated and sometimes gets into a cyclic pattern of switching from one point of the flowfield to the neighboring points. This can happen especially in the region above the shock in the field where the shock is weakening. In some cases this produces a maximum residual which is large at those points and gives the total residual an appearance of nonconvergence. Varying the values of the dissipation coefficients ϵ_e and ϵ_i can help, but not always. Therefore, this scheme is not recommended and has been abandoned at least until a better parameter scheme is found.

VII. Nonlinear Artificial Dissipation

The occurrence of the oscillations at the shocks for the preceding schemes can be traced to the problem of differencing across the shock where too big of a differencing stencil is employed. In the case of the fourth-difference dissipation, oscillations are controlled in the smooth regions of the flow quite well but at the shock the high-frequency oscillations occur, as shown in Fig. 1. Consider the linear problem

$$u_t+u_x=0 \tag{24}$$

solved on a finite difference mesh $u_j^n=u(j\Delta x,n\Delta t)$ with the initial conditions (representing a discontinuity at grid point J)

$$u_j^n=\begin{cases}1, & j\le J-1\\ 0, & j=J\\ -1, & j\ge J+1\end{cases} \tag{25}$$

Taking $\Delta x=\Delta t=1$ represents a Courant number of 1. Given this initial condition, propagate the solution one time step with the scheme

$$u_j^{n+1}=u_j^n-\frac{(u_{j+1}^n-u_{j-1}^n)}{2}+f_j \tag{26}$$

The function f_j will be two different dissipation terms based on the operators defined in Eqs. (18). Let

$$f_j=\begin{cases}f_j^{(4)}=-\tfrac{1}{4}(u_{j+2}^n-4u_{j+1}^n+6u_j^n-4u_{j-1}^n+u_{j-2}^n)\\ f_j^{(2)}=\tfrac{1}{2}(u_{j+1}^n-2u_j^n+u_{j-1}^n)\end{cases} \tag{27}$$

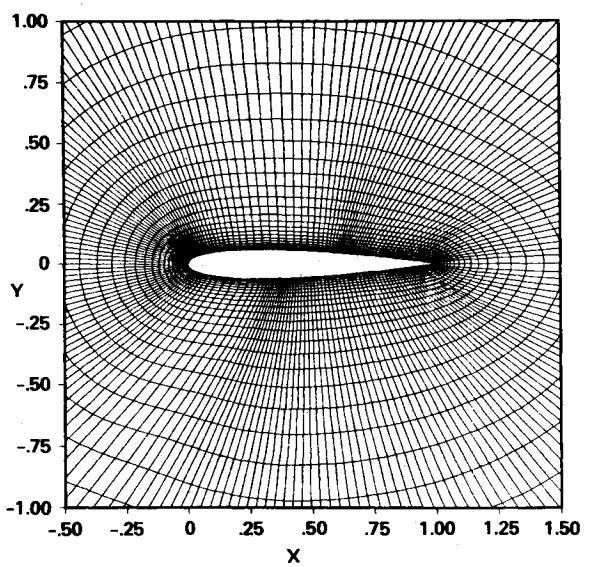

Fig. 3 Clustered grid for NACA 0012 airfoil.

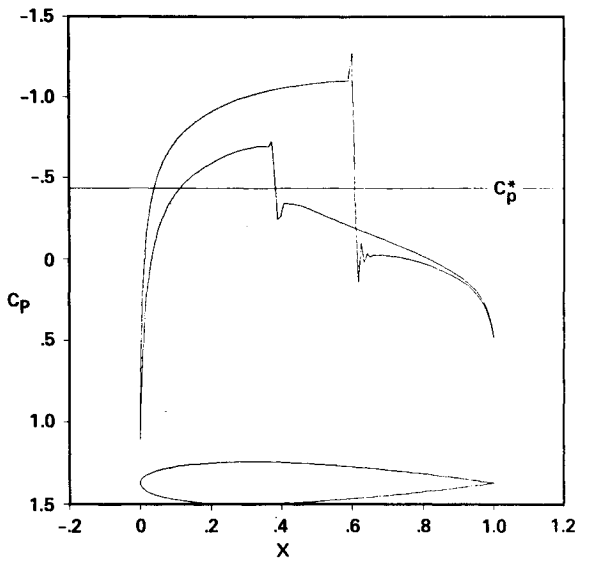

Fig. 4 Coefficient of pressure for central-upwind solution.

Using the fourth-difference dissipation $f_j^{(4)}$, the solution after one step becomes

$$u_j^{n+1} = \begin{cases} 1, & j \le J-3 \\ 5/4, & j = J-2 \\ 1, & j = J-1 \\ 1, & j = J \\ 0, & j = J+1 \\ -5/4, & j = J+2 \\ -1 & j \ge J+3 \end{cases} \tag{28}$$

while the second-difference dissipation $f_j^{(2)}$ produces

$$u_j^{n+1} = \begin{cases} 1, & j \le J \\ 0, & j = J+1 \\ -1, & j \ge J+2 \end{cases} \tag{29}$$

Comparing Eqs. (28) and (29) with the initial condition equation (25), the second-difference dissipation allows the initial condition to propagate exactly while the fourth-difference term produces an overshoot before the shock and undershoot after. This is a direct result of the five-point differencing stencil across the shock. As shown above, the second-difference dissipation combined with central differences produces first-order spatial accuracy. In general, the loss in accuracy is undesirable. To maintain spatial second-order accuracy, the fourth-difference dissipation terms are usually used everywhere except for the use of second-difference dissipation in regions near shocks or discontinuities.

MacCormack and Baldwin[19] employed a second-difference dissipation operator in the solution of the Navier-Stokes equations for flow with shocks. The dissipation model

$$\Delta t \frac{\partial}{\partial x}\left(\frac{|u|+a}{4p}\left|\frac{\partial^2 p}{\partial x^2}\right|\frac{\partial Q}{\partial x}\right) \tag{30}$$

was added to the explicit algorithm in Cartesian coordinates. The coefficient for the dissipation terms based on the local pressure gradient enhances the model's ability to capture shocks and eliminate oscillations. Equation (30) is a second-difference form, although it can be argued that in smooth regions $\partial^2 p/\partial x^2$ is second-order and therefore the total term is a fourth-difference. Note two things about Eq. (30): the scaling by Δt for consistency in the steady state and the scaling by $|u|+a$, which is similar to the $|A|$ seen in Eqs. (18). In fact, in Cartesian coordinates $|u|+a$ is the spectral radius of $|A|$.

Jameson et al.[4] has employed a similar dissipative model combined with a fourth-difference term. The model rewritten in our notation is

$$\nabla_\xi (\sigma_{j+1,k} J^{-1}_{j+1,k} + \sigma_{j,k} J^{-1}_{j,k}) (\epsilon^{(2)}_{j,k} \Delta_\xi Q_{j,k} - \epsilon^{(4)}_{j,k} \Delta_\xi \nabla_\xi \Delta_\xi Q_{j,k}) \tag{31}$$

with

$$\epsilon^{(2)}_{j,k} = \kappa_2 \Delta t \max(\Upsilon_{j+1,k}, \Upsilon_{j,k}, \Upsilon_{j-1,k})$$

$$\epsilon^{(4)}_{j,k} = \max_j(0, \kappa_4 \Delta t - \epsilon^{(2)}_{j,k})$$

where typical values of the constants are $\kappa_2 = 1/4$ and $\kappa_4 = 1/100$ and the maximum function is used to spread the second-difference dissipations range over a few grid points. Similar terms are used in the η direction. The coefficient to the second-difference dissipation Υ at the point j,k is

$$\Upsilon_{j,k} = \frac{|p_{j+1,k} - 2p_{j,k} + p_{j-1,k}|}{|p_{j+1,k} + 2p_{j,k} + p_{j-1,k}|}$$

which is similar to the $\partial^2 p/\partial x^2$ term in Eq. (30). The term $\sigma_{j,k}$ is a spectral radius scaling and in two-dimensions is defined as

$$\sigma_{j,k} = |U| + a\sqrt{\xi_x^2 + \xi_y^2} + |V| + a\sqrt{\eta_x^2 + \eta_y^2}$$

which is a sum of the spectral radii of A and B.

The first term of Eq. (31) is a second-difference dissipation with an extra pressure gradient coefficient to increase its value near shocks. Note that this term has a very similar form to Eq. (30). The second term is a fourth-difference term, where the logic to compute $\epsilon^{(4)}_{j,k}$ switches it off when the second-difference nonlinear coefficient is larger than the constant fourth-difference coefficient. This occurs right near a shock. This model has been implemented in the solution algorithm. It is added to the right-hand side of the algorithm in place of $D^{(4)}$ in Eq. (20b) and applied to the test problem of Fig. 1. Results are shown in Figs. 6 and 7. These results

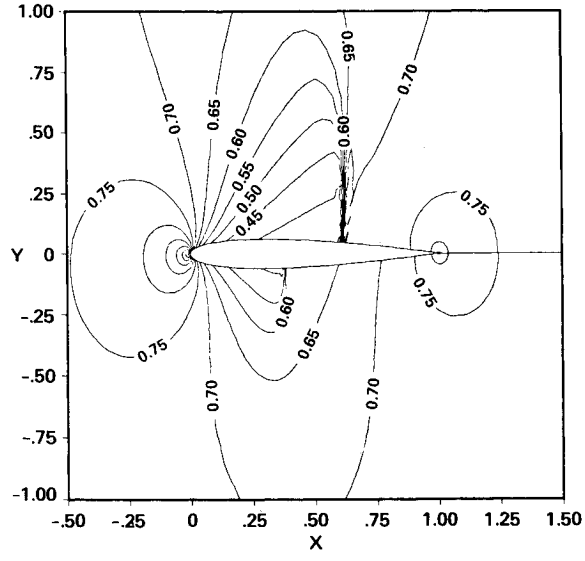

Fig. 5 Pressure field showing extent of oscillations.

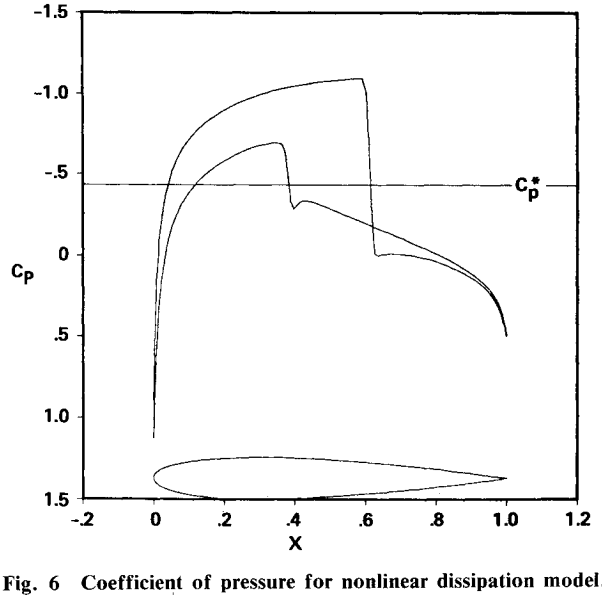

Fig. 6 Coefficient of pressure for nonlinear dissipation model.

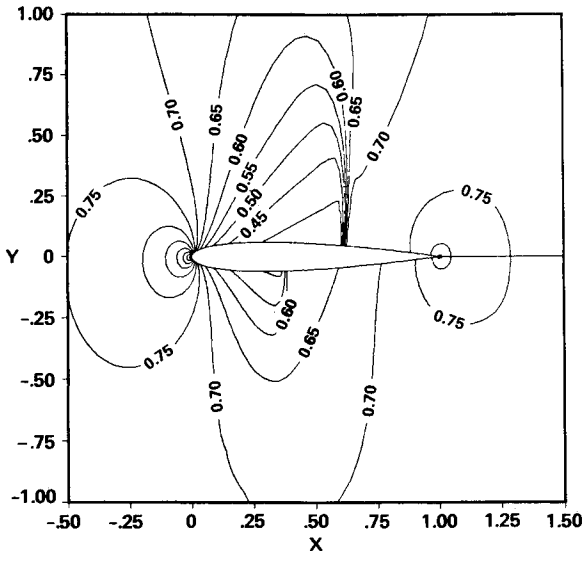

Fig. 7 Pressure field for nonliniear dissipation model.

show a marked improvement in the ability to capture the shocks without introducing oscillations. The shocks are still quite sharp and the overall solutions are quite good. Similar results can be obtained for a wide variety of cases. An example can be found in Ref. 20, where highly accurate solutions using the nonlinear dissipation are contrasted with solutions using the upwind plus central scheme described in Sec. VI.

VIII. Analysis of Dissipation Operators for an Implicit Algorithm

As discussed in Sec. V, based on linear theory the use of explicit dissipation produces an explicit stability bounds unless implicit dissipation is added. The second-difference dissipation, Eq. (20b), will stabilize the fourth-difference dissipation if the coefficients are chosen properly. Ideally though, it would be better to treat the explicit dissipation in a fully implicit manner. That is, use implicit fourth-difference dissipation which is an exact linearization of the explicit fourth-difference dissipation. In fact, although the implicit second-difference dissipation stabilizes the fourth-difference dissipation it can have a detrimental effect on the convergence rates of an implicit algorithm for steady-state computations.

Consider the model problem in one-dimension,

$$q_t + aq_x = 0 \tag{32}$$

where a represents an eigenvalue of A. Applying a first-order time accurate delta implicit scheme to Eq. (32) and adding explicit fourth-difference dissipation ($\beta_4 > 0$), implicit second-difference dissipation ($\alpha_2 > 0$), and implicit fourth-difference dissipation ($\alpha_4 > 0$) gives the algorithm

$$[1 + ha\delta_x - h\alpha_2 \nabla_x \Delta_x + h\alpha_4 (\nabla_x \Delta_x)^2](q^{n+1} - q^n)$$
$$= -h[a\delta_x + \beta_4 (\nabla_x \Delta_x)^2] q^n \tag{33}$$

Fourier analysis using $q^n = w^n e^{ikj\Delta x}$ (with k_j the wave number in x) produces

$$[1 + ha\lambda_x - h\alpha_2 \mu_x + h\alpha_4 \mu_x^2](w^{n+1} - w^n) = -h(a\lambda_x + \beta_4 \mu_x^2) w^n \tag{34}$$

where $\lambda_x = 2i\sin(k_j \Delta x)/\Delta x$ represents the Fourier signature for the central difference δ_x, $\mu_x = -2 + 2\cos(k_j \Delta x)$ the signature of the second-difference dissipation operator $\nabla_x \Delta_x$, and μ_x^2 for the fourth-difference dissipation.

The amplification factor for $w^{n+1} = \sigma w^n$ is then

$$\sigma = \frac{1 + h[(\alpha_4 - \beta_4)\mu_x^2 - \alpha_2 \mu_x]}{1 + h(\lambda_x - \alpha_2 \mu_x + \alpha_4 \mu_x^2)} \tag{35}$$

The choices that will be investigated are as follows:

1) $\beta_4 \neq 0$ and $\alpha_4 = \alpha_2 = 0$, explicit dissipation only.

2) $\beta_4 \neq 0$, $\alpha_2 \neq 0$, and $\alpha_4 = 0$, explicit fourth-difference dissipation and implicit second-difference dissipation, no implicit fourth-difference dissipation.

3) $\beta_4 \neq 0$, $\alpha_4 \neq 0$, and $\alpha_2 = 0$, explicit and implicit fourth-difference dissipation with no implicit second-difference dissipation.

For case 1, explicit dissipation only, Eq. (35) becomes

$$\sigma = \frac{1 - h\beta_4 \mu_x^2}{1 + h\lambda_x} \tag{36a}$$

Now, since λ_x is pure imaginary and has a minimum of 0, and $-4 \leq \mu_x \leq 0$, the explicit stability bound is $h\beta_4 < \frac{1}{8}$. This is a limit on the product of h and β_4 and therefore one can always find a combination which will be stable. But, for arbitrary h, especially in the case where large h is used to accelerate convergence, this boundary is too restrictive.

In the second case, implicit second-difference dissipation can eliminate the above stability bound. The amplification factor σ is now

$$\sigma = \frac{1 - h\beta_4 \mu_x^2 - h\alpha_2 \mu_x}{1 + h\lambda_x - h\alpha_2 \mu_x} \tag{36b}$$

The denominator term λ_x can only improve the stability bounds since it is pure imaginary, so it is taken at its minimum, 0. Let $\alpha_2 = 2\beta_4$ and apply the stability condition $|\sigma| \leq 1$ which results in the condition $-2 \leq -h\beta_4 \mu_x (4 + \mu_x)$. Since $\mu_x \leq 0$, the condition can be rewritten as $-2 \leq h\beta_4 |\mu_x| (4 + \mu_x)$ which is satisfied because $-4 \leq \mu_x$. Therefore, using $\alpha_2 = 2\beta_4$ leads to unconditional stability. The disadvantage of this form is evident from the amplification factor, Eq. (36b). Even though the scheme is unconditionally stable, $\sigma \to 1$ as $h \to \infty$. In fact, the amplification factor has a minimum at a finite h and then asymptotes rapidly to 1 as h increases. For this reason, large h cannot be used to accelerate convergence even in this simple one-dimensional example.

In contrast, the third case of implicit and explicit dissipation is unconditionally stable and has good convergence characteristics for large h. The amplification factor σ for $\alpha_4 = \beta_4$ and $\alpha_2 = 0$ is

$$\sigma = \frac{1}{1 + h(\lambda_x + \alpha_4 \mu_x^2)} \tag{36c}$$

which is unconditionally stable and $\sigma \to 0$ as $h \to \infty$.

The analysis for two and three dimensions is similar, except that implicit factorizations interfere with the large time step convergence characteristics (see Ref. 11).

IX. Implicit Fourth-Difference Dissipation

A fully implicit treatment of the fourth-difference artificial dissipation would significantly increase the computational work and storage requirements of the full block algorithm. The solution of Eqs. (19) and (20) requires the inversion of block tridiagonal matrices. If fully implicit fourth-difference dissipation were used, then block pentadiagonal inversions would be necessary, which would greatly increase the computational cost of the algorithm.

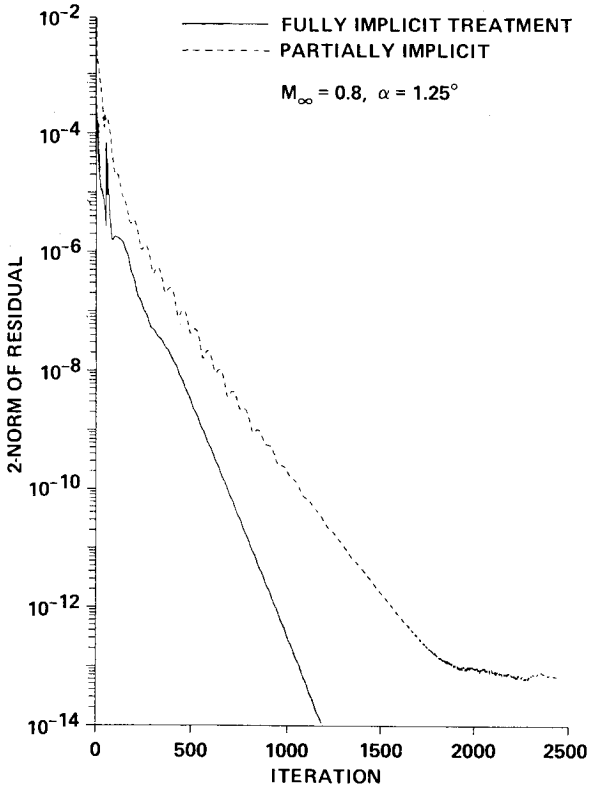

Fig. 8 Improvement in convergence due to implicit treatment of nonlinear dissipation terms.

A variation of the implicit approximation factorization algorithm equation (19) due to Pulliam and Chaussee[21] can be used to reduce substantially this computational cost, especially for the implict fourth-difference dissipation. The new algorithm diagonalizes the implicit operators, which makes the use of implicit dissipation practical.

The left-hand side of the numerical method in Eq. (19) is modified to

$$T_\xi [I + h\delta_\xi \Lambda_\xi] \hat{N} [I + h\delta_\eta \Lambda_\eta] T_\eta^{-1} \Delta \hat{Q}^n = \hat{R}^n \tag{37}$$

where $\hat{N} = T_\xi^{-1} T_\eta$, $\Delta \hat{Q}^n = \hat{Q}^{n+1} - \hat{Q}^n$, $h = \Delta t$ and T_ξ, T_η are the eigenvector matrices for the flux Jacobians $\hat{A}$ and $\hat{B}$ (i.e., $\hat{A} = \partial \hat{E}/\partial \hat{Q}$). Computational work is reduced because this scheme requires the solution of scalar tridiagonals instead of the block tridiagonals needed for Eq. (19).

The fourth-difference dissipation is added directly to the diagonal elements of Eq. (37) for each of the implicit operators. The cost of pentadiagonal inversion is greatly reduced over the block form since now only scalar pentadiagonals are needed. In fact, the computational cost of the pentadiagonal algorithm is even less than the original block tridiagonal system. The net effect is enhanced convergence and stability with a minimal increase in cost.

Treating the fourth-difference nonlinear dissipation operators, Eq. (31) implicitly in the diagonal algorithm gives the altered form

$$T_\xi [I + h\delta_\xi \Lambda_\xi - hD_i|_\xi] \hat{N} [I + h\delta_\eta \Lambda_\eta - hD_i|_\eta] T_\eta^{-1} \Delta \hat{Q}^n = \hat{R}^n \tag{38}$$

where the D_i are redefined as

$$D_i|_\xi = \nabla_\xi (\sigma_{j+1,k} J_{j+1,k}^{-1} + \sigma_{j,k} J_{j,k}^{-1})(\epsilon_{j,k}^{(2)} \Delta_\xi - \epsilon_{j,k}^{(4)} \Delta_\xi \nabla_\xi \Delta_\xi) J$$

Terms for $D_i|_\eta$ have a similar form. The nonlinear coefficients are not linearized since they are rather complicated functions of Q.

The effectiveness of treating the fourth-difference terms implicitly in the NACA 0012 test case in indicated by Fig. 8. Shown here are results using the constant coefficient explicit nonlinear dissipation, with implicit second-difference constant coefficient dissipation [Eqs. (19) and (20)] compared to the fully implicit treatment [Eqs. (37) and (38)]. Fully implicit treatment of the numerical dissipation improves convergence and also improves the robustness of the algorithm. In general, the practical stability limits of the codes are increased with implicit treatment of the dissipations.

X. Boundary Approximations for Dissipation Operators

The dissipation operators introduced in the preceding sections all employed at least three-point and usually five-point differencing stencils. In the interior of a flowfield grid this does not pose any problem. The question arises though as to the application at and near the boundaries of the domains. Typically, in finite difference calculations one does not solve the flowfield equations at the boundaries. The values at the boundaries are either obtained from some fixed conditions or calculated from a boundary procedure such as extrapolations or separate boundary equations. It will be assumed for most of this presentation that dissipation formulas are only needed at the points adjacent to the boundaries and not at the boundaries themselves.

One procedure used with the constant coefficient dissipation, Eq. (20a), is to drop the fourth-difference terms ($\nabla\Delta\nabla\Delta$) to a second-difference stencil ($\nabla\Delta$) at the boundaries. This is a local error and does not affect the overall accuracy.

Eriksson and Rizzi[22] suggest a procedure for choosing and evaluating dissipation boundary schemes. The constraint on the operators is that no points from outside the solution domain are used. This requires that noncentered difference operators be used at the boundaries. If the dissipation operator including the boundary treatment is represented as the matrix operator Du_j then the operator is fully dissipative if D is nonpositive definite. This can be shown for arbitrary D by showing that

$$u^T D u = \sum_{j=1}^{NJ} u_j D u_j \le 0 \tag{39}$$

where NJ is the total number of points in j. Let the matrix D be defined as the five-point central scheme in the interior, $3 \le j \le NJ-2$,

$$-(\nabla_x \Delta_x)^2 u_j = -u_{j+2} + 4u_{j+1} - 6u_j + 4u_{j-1} - u_{j-2} \tag{40a}$$

and the boundary equations,

$$\text{at } j=1\text{: } \alpha_3 u_3 + \alpha_2 u_2 + \alpha_1 u_1$$

$$\text{at } j=2\text{: } \beta_4 u_4 + \beta_3 u_3 + \beta_2 u_2 + \beta_1 u_1 \tag{40b}$$

with similar formulas at the other boundaries, $j = NJ-1$, NJ. Applying Eqs. (40a) and (40b) to Eq. (39), coefficients α_i and β_i can be found which ensure a quadratic form such that

$$u^T D u = -\sum_{j=2}^{NJ-1} (u_{j+1} - 2u_j + u_{j-1})^2 \le 0 \tag{41}$$

and therefore D is nonpositive definite. The coefficients are

$$\alpha_3 = -1, \quad \alpha_2 = 2, \quad \alpha_1 = -1$$

$$\beta_4 = -1, \quad \beta_3 = 4, \quad \beta_2 = -5, \quad \beta_1 = 2 \tag{42}$$

The two equations defined by these coefficients and Eq. (40b) are second-difference dissipation terms. These equations can be applied right up to the boundary point $j=1$, but in typical finite difference calculations only the second formula is used at grid point $j=2$.

One way to analyze different dissipation operators is to form the associated matrices for a finite number of points and use computer software to compute the eigenvalues which then can be used to quantify the dissipative nature of each scheme. While this type of analysis is by no means rigorous or general it does provide at least a first-order measure. For the dissipation operator of Eqs. (40) the matrix D is

$$\begin{bmatrix} -1 & 2 & -1 & & & & & & & \\ 2 & -5 & 4 & -1 & & & & & & \\ -1 & 4 & -6 & 4 & -1 & & & & & \\ & -1 & 4 & -6 & 4 & -1 & & & & \\ & & -1 & 4 & -6 & 4 & -1 & & & \\ & & & -1 & 4 & -6 & 4 & -1 & & \\ & & & & -1 & 4 & -6 & 4 & -1 & \\ & & & & & -1 & 4 & -5 & 2 & \\ & & & & & & -1 & 2 & -1 & \end{bmatrix} \tag{43a}$$

The eigenvalues of this 10×10 matrix are as follows:

i	λ_i	i	λ_i
1	−0.00000	6	−3.16286
2	−0.00000	7	−5.96245
3	−0.05053	8	−9.36075
4	−0.36889	9	−12.67808
5	−1.30896	10	−15.10753

which are all negative except for two zeros.

Excluding the boundary equations, $j=1,NJ$ gives

$$\begin{bmatrix} -5 & 4 & -1 & & & & & & \\ 4 & -6 & 4 & -1 & & & & & \\ -1 & 4 & -6 & 4 & -1 & & & & \\ & -1 & 4 & -6 & 4 & -1 & & & \\ & & -1 & 4 & -6 & 4 & -1 & & \\ & & & -1 & 4 & -6 & 4 & -1 & \\ & & & & -1 & 4 & -6 & 4 & \\ & & & & & -1 & 4 & -5 & \end{bmatrix} \tag{43b}$$

which has the all negative eigenvalues

i	λ_i	i	λ_i
1	−0.01455	5	−5.50980
2	−0.21894	6	−9.00000
3	−1.00000	7	−12.47565
4	−2.73143	8	−15.04964

This is the form of the operator used at the boundaries for the calculations performed using the nonlinear dissipation operators, Eq. (31). It is fully dissipative and has proven to be reliable and robust.

Another form that was discussed previously is the second-difference formula at $j=2$, $NJ-1$ with the fourth-difference interior,

$$\begin{bmatrix} -2 & 1 & & & & & & & \\ 4 & -6 & 4 & -1 & & & & & \\ -1 & 4 & -6 & 4 & -1 & & & & \\ & -1 & 4 & -6 & 4 & -1 & & & \\ & & -1 & 4 & -6 & 4 & -1 & & \\ & & & -1 & 4 & -6 & 4 & -1 & \\ & & & & -1 & 4 & -6 & 4 & \\ & & & & & -1 & 4 & -6 & \end{bmatrix} \tag{43c}$$

which again has all negative eigenvalues

i	λ_i	i	λ_i
1	−0.02345	5	−3.82420
2	−0.30375	6	−7.05489
3	−1.00000	7	−11.15236
4	−2.00923	8	−14.63214

This boundary treatment appears less dissipative at the high-frequency end and more dissipative at the low-frequency end of the spectrum than the previous method.

Finally, a form that has seen some use is a four-point one-sided stencil at $j=2$ and $j=NJ-1$,

$$\begin{bmatrix} -3 & 3 & -1 & & & & & & \\ 4 & -6 & 4 & -1 & & & & & \\ -1 & 4 & -6 & 4 & -1 & & & & \\ & -1 & 4 & -6 & 4 & -1 & & & \\ & & -1 & 4 & -6 & 4 & -1 & & \\ & & & -1 & 4 & -6 & 4 & -1 & \\ & & & & -1 & 4 & -6 & 4 & \\ & & & & & -1 & 3 & -3 & \end{bmatrix} \tag{43d}$$

which again has all negative eigenvalues

i	λ_i	i	λ_i
1	−0.00000	5	−4.51280
2	−0.07717	6	−8.10273
3	−0.55723	7	−11.92997
4	−1.93387	8	−14.88625

except for the one zero. Forms with zero eigenvalues are not recommended since they may lead to undamped modes which could cause instabilities.

All of the above boundary treatments for the dissipation operators have proven to be successful in practical computations although the formulas used for Eq. (43b) seem to produce the least detrimental effect on the accuracy of practical compositions.

XI. Summary

Numerical dissipation operators can be combined with central differencing to produce accurate, stable, and robust algorithms. The solutions obtained can be oscillation free and still capture shocks sharply independent of mesh clustering. In numerious computational applications, the combination of the nonlinear dissipation equation (31) and its im-

plicit treatment, Eq. (38), has proven to give very accurate, stable, and reliable solutions for a wide range of flowfields from transonic inviscid airfoils to Navier-Stokes solutions for an airfoil with a deployed spoiler.[23] Proper boundary formulas for the fourth-difference dissipation can be found which assure a dissipative operator.

The dissipation models discussed here have been extended to three-dimensions in a straightforward fashion and have resulted in substantial increases in accuracy, efficiency, and robustness in a number of examples.

References

[1]MacCormack, R. W., "The Effect of Viscosity in Hypervelocity Impact Cratering," AIAA Paper 69-354, 1969.

[2]Steger, J. L., "Implicit Finite Difference Simulation of Flow About Arbitrary Geometries with Application to Airfoils," *AIAA Journal*, Vol. 16, July 1978, p. 679.

[3]Beam, R. and Warming, R. F., "An Implicit Finite-Difference Algorithm for Hyperbolic Systems in Conservation Law Form," *Journal of Computational Physics*, Vol. 22, Sept. 1976, pp. 87-110.

[4]Jameson, A., Schmidt, W., and Turkel, E., "Numerical Solutions of the Euler Equations by Finite Volume Methods Using Runge-Kutta Time-Stepping Schemes," AIAA Paper 81-1259, 1981.

[5]Rizzi, A. and Eriksson, L., "Explicit Multistage Finite Volume Procedure to Solve the Euler Equations for Transonic Flow," *Lecture Series on Computational Fluid Dynamics*, von Kármán Institute, Rhode-St-Genese, Belgium, 1983.

[6]Steger, J. L. and Warming, R. F., "Flux Vector Splitting of the Inviscid Gas Dynamic Equations with Applications to Finite Difference Methods," *Journal of Computational Physics*, Vol. 40, April 1981, pp. 263-293.

[7]Roe, P. L., "The Use of the Riemann Problem in Finite Difference Schemes," *Seventh International Conference on Numerical Methods in Fluid Dynamics*, Stanford, CA, 1980.

[8]Van Leer, B., "Flux-Vector Splitting for the Euler Equations," *Eighth International Conference on Numerical Methods in Fluid Dynamics, Springer Lecture Notes in Physics No. 170*, edited by E. Krause, 1983.

[9]Osher, S. and Chakravarthy, S., "Upwind Schemes and Boundary Conditions with Applications to Euler Equations in General Geometries," *Journal of Computational Physics*, Vol. 50, 1983, pp. 447-481.

[10]Harten, A., "A High Resolution Scheme for the Computation of Weak Solutions of Hyperbolic Conservation Laws," *Journal of Computational Physics*, Vol. 49, 1983, pp. 357-393.

[11]Pulliam, T., "Euler and Thin Layer Navier-Stokes Codes: ARC2D, ARC3D," *Notes for Computational Dynamics User's Workship,* UTSI E02-4005-023-84, March 1984.

[12]Pulliam, T. H. and Steger, J. L., "Recent Improvements in Efficiency, Accuracy, and Convergence for Implicit Approximate Factorization Algorithms," AIAA Paper 85-0360, Jan. 1985.

[13]Warming, R. F., Beam, R., and Hyett, B. J., "Diagonalization and Simultaneous Symmetrization of the Gas-Dynamic Matrices," *Mathematics of Computation*, Vol. 29, Oct. 1975, p. 1037.

[14]Liu, Y., "A Nonstationary Relaxation Technique for Solving the Equations of Gas Dynamics," Ph.D. Dissertation, Stanford University, Stanford, CA, March 1984.

[15]Liu, Y. and Lomax, H., "A Nonstationary Relaxation Method for the Cauchy-Riemann and 1-D Euler Equations," AIAA Paper 83-1905, June 1983.

[16]Von Neumann, J. and Richtmyer, R. D., "A Method for the Numerical Calculation of Hydrodynamic Shocks," *Journal of Applied Physics*, Vol. 21, March 1950, pp. 232-237.

[17]Warming, R. and Beam, R., "On the Construction and Application of Implicit Factored Schemes for Conservation Laws," *SIAM-AMS Proceedings*, Vol. 11, 1978, pp. 85-129.

[18]Pulliam, T. H., Jespersen, D. C., and Childs, R. E., "An Enhanced Version of an Implicit Code for the Euler Equations," AIAA Paper 83-0344, 1983.

[19]MacCormack, R. and Baldwin, B., "A Numerical Method for Solving the Navier-Stokes Equations with Application to Shock Boundary Layer Interactions," AIAA Paper 75-1, 1975.

[20]Pulliam, T. H. and Barton, J. T., "Euler Computations of AGARD Working Group 07 Airfoil Test Cases," AIAA Paper 85-0018, 1985.

[21]Pulliam T. H. and Chaussee, D. S., "A Diagonal Form of an Implicit Approximate Factorization Algorithm," *Journal of Computational Physics*, Vol. 39, 1981.

[22]Eriksson, L. E., and Rizzi, A., "Analysis by Computer of the Convergence to Steady State of Discrete Approximations to the Euler Equations," AIAA Paper 83-1951, 1983.

[23]Barth, T. and Pulliam, T. H., "Navier-Stokes Computations for Exotic Airfoils," AIAA Paper 85-0109, Jan. 1985.